Model of the plasma discharge in a Hall thruster with heat conduction

E. Ahedo and J. M. Gallardo
E.T.S.I. Aeronáuticos, Universidad Politécnica, 28040 Madrid, Spain

M. Martínez-Sánchez
Massachusetts Institute of Technology, Cambridge, Massachusetts 02139

(Received 15 April 2002; accepted 14 June 2002)

The inclusion of heat conduction into a one-dimensional, macroscopic model of the plasma inside a Hall thruster and in the near plume is found to smooth the temperature profile of previous solutions with a nonconductive model. The spatial structure still consists of reverse-flow, ionization, and acceleration regions. Conductive energy flow, being of the same order of convective flow, has significant effects on the rear part of the channel where it can make impossible the establishment of a steady anode sheath. As a result, there is an upper bound on the plasma reverse flow for the existence of stationary solutions. The analysis of inertial effects on the electron dynamics concludes that the main contribution is the azimuthal electron motion, which can produce extra collisionality, mainly in the near plume. The different contributions to the effective axial diffusion of electrons and the ion temperature are evaluated. A parametric investigation yields the basic scaling laws of the thruster stationary performance. © *2002 American Institute of Physics.*
[DOI: 10.1063/1.1499496]

I. INTRODUCTION

Recently we presented a one-dimensional (1D) model (hereafter called Model I) of the stationary axial structure of the plasma discharge inside a Hall thruster and in the near plume.[1] The structure consisted in an anode sheath, a region of free diffusion for electrons and reverse flow for ions, the ionization layer, and the acceleration region, which extends into the plume, Fig. 1. Although quantitative accuracy could not be expected from Model I, it reproduced rather well most of the main features of the experimental data.[2–6] Compared to previous 1D models,[7–9] Model I unveiled the combined importance of the electron pressure and the reverse flow of ions in shaping the plasma structure. In addition, the inclusion of the near plume (with the neutralization surface) allowed closure of the formulation with realistic boundary conditions, and parametric studies on thruster performance. Of particular interest was the determination of the parametric domain of stationary solutions of the model, which was bounded by the case of zero ion reverse flow.[10,11]

The main defect of Model I came from the simplified treatment of the electron energy equation, which included neither heat conduction nor the losses coming from the interaction with the lateral walls of the chamber. The resulting temperature profile had too large gradients around the ionization region and too large a peak temperature. A hybrid (particle/fluid) numerical model by Fife, which includes heat conduction and wall losses, yields smoother temperature profiles.[12] In this paper we present a 1D macroscopic model (hereafter called Model II) which adds heat conduction to Model I. The first point to be emphasized is that heat conduction is not a new forcing term added to the equations of Model I: it transforms the electron energy equation from first to second order for the electron temperature, a fact having major implications in the mathematical treatment and the parametric domain of stationary solutions. The effects of the plasma interaction with lateral walls are not included in Model II. There are two reasons: first, a detailed radial model of that interaction, to be coupled to the axial model, is still under investigation;[13] and second, it is of interest to understand the plasma response in thrusters where lateral losses are small.

The paper includes the detailed formulation of Model II, the discussion of the spatial response, and a parametric investigation on the thruster stationary performance. In addition, three issues, not treated in detail in Ref. 1, are analyzed here. The first one, treated more or less explicitly in the recent literature, is the evaluation of the collisional approximation for the electron motion. Tahara *et al.*[14] and Barral *et al.*[15] have added different inertial terms into their 1D macroscopic models; Fedotov *et al.*[16] suggest the presence of unmagnetized and magnetized populations of electrons near the thruster exit; Haas and Gallimore[6] conclude, from their experiments, that the azimuthal drift energy can be high enough to contribute to ionization. The second issue is the computation of the ion temperature, seeking a confirmation that it can be neglected everywhere compared to either the electron temperature or the ion beam velocity. And the third one is a detailed evaluation of the thrust: computations based on the momentum thrust of the plasma either at the channel exhaust (as we did in Ref. 1), or in the far plume (as simulation models usually do[12]) are not accurate enough.

The paper is organized as follows. In Sec. II we formulate the quasineutral model, including a detailed discussion on the collisional approximation for electrons. In Sec. III we discuss the model singular points, the anode sheath, the boundary conditions, and the numerical procedure. In Sec. IV we analyze the spatial solution, and we evaluate the different collision frequencies and the ion temperature. In Sec.

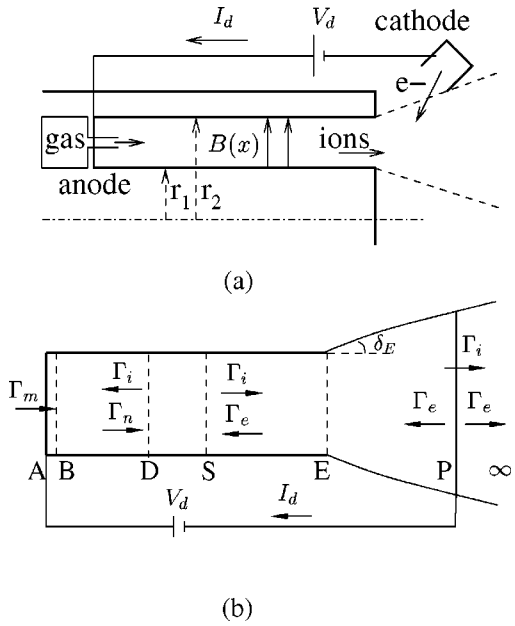

FIG. 1. Sketches of (a) the Hall thruster, and (b) the axial model. $\Gamma_\alpha = A_c n_\alpha v_{x\alpha}$, $\alpha = i,e,\ldots$ are axial flows of particles of the different species. Point A is the anode, point B is the anode sheath transition, point E is the exit of the thruster chamber, and point P is the neutralization surface. Points D and S are the zero-velocity and forward-sonic points of the ion flow, respectively, and can be taken as the practical boundaries of the ionization region.

V we derive the different contributions to the thrust and the thrust efficiency. In Sec. VI we discuss the thruster performance in the parametric domain of stationary solutions. Conclusions are written in Sec. VII.

II. THE QUASINEUTRAL MODEL

Geometrical sketches of the thruster and the axial model are drawn in Figs. 1(a) and 1(b). The general hypotheses of the present Model II are the same as in Model I. In the 1D axial approximation, plasma variables represent average values on each cross section and depend only on the axial variable x. The macroscopic formulation consists of fluid-like equations for ions (i), electrons (e), and neutrals (n). The thruster channel is of length L_c, radial area A_c, and radial width h_c. The plasma discharge extends outside the thruster into a plasma plume of radial area $A(x)$ to be determined. The magnetic field is considered purely radial, $\mathbf{B}=B(x)\mathbf{1}_r$, with the maximum field $B_{\max}$ placed near the thruster exit, and two different semi-Gaussian axial profiles are used inside the thruster and in the near plume. Electrons are injected into the plume at a neutralization surface (point P) placed at a distance L_{cat} from the channel exit (point E). The voltage difference between anode (point A) and point P is the discharge voltage, V_d, and the electron current delivered at the neutralization surface is the discharge current, I_d. One part of this current flows outwards and neutralizes the ion beam current there, I_{iP}; the other part, $I_d - I_{iP}$, diffuses inwards across the radial lines of the applied magnetic field and ionizes the mass flow of neutrals, $\dot{m}_A$, injected at the anode; subscript ∞ will refer to downstream conditions far away from the cathode P. No effects of the radial interaction of the plasma with the lateral walls of the chamber are included here.

The axial plasma flow is considered quasineutral everywhere except in a thin, electron-repelling sheath attached to the anode (region AB in Fig. 1, with $x_B \simeq x_A = 0$ in the quasineutral scale). The potential jump in the sheath, $\phi_{AB} = \phi_B - \phi_A > 0$, adjusts the small diffusive electron flow in the channel to the thermal flow collected at the anode. Assuming the anode does not emit ions and the ionization region is not tied to the anode, a region of reverse ion flow must exist in the rear part of the channel (region BD in Fig. 1).

A. Electron dynamics

We review here the closed-drift, collisional model for the electrons in order to evaluate the importance of inertial effects. Also, the equation for electron heat conduction is formulated.

The vector equation for the electron momentum is

$$m_e n_e \mathbf{v}_e \cdot \nabla \mathbf{v}_e = -\nabla n_e T_e + e n_e \nabla \phi - e n_e \mathbf{v}_e \wedge \mathbf{B} - \mathbf{R}_e . \quad (1)$$

Apart from conventional symbols,

$$\mathbf{R}_e = m_e n_e (\nu_e \mathbf{v}_e - \nu_{ei}\mathbf{v}_i - \nu_{en}\mathbf{v}_n)$$

is the friction force due to collisions, with $\nu_e = \nu_{en} + \nu_{ei} + \nu_{\text{ano}}$, the total collision frequency for electrons. This includes contributions from electron–neutral collisions (ν_{en}), electron–ion collisions (ν_{ei}), and anomalous effective collisions representing Bohm-type diffusion, which is expressed as $\nu_{\text{ano}} = \alpha_{\text{ano}}\omega_e$, with $\omega_e = eB/m_e$ the electron gyrofrequency and α_{ano} a parameter with a classical value of 1/16.[17] The presence of an anomalous diffusion was already reported by Janes and Lowder[2] who attributed it to observed correlated density and electric field azimuthal fluctuations. When current losses to lateral walls are taken into account, ν_e has another contribution from electron exchanges at the walls.[13,18]

In the 1D axial approximation, the electron velocity field is $\mathbf{v}_e = v_{xe}\mathbf{1}_x + v_{\theta e}\mathbf{1}_\theta$, and spatial gradients reduce to the axial direction, $\nabla \equiv \mathbf{1}_x d/dx$. Then, applying the closed-drift hypothesis,

$$\omega_e \gg \nu_e , \quad (2)$$

and the ansatz $|v_{\theta e}/v_{xe}| \sim \omega_e/\nu_e$, Eq. (1) simplifies into

$$0 \simeq m_e n_e \omega_e v_{\theta e} - d(n_e T_e)/dx + e n_e \, d\phi/dx, \quad (3)$$

$$v_{xe}\, dv_{\theta e}/dx \simeq -\omega_e v_{xe} - \nu_e v_{\theta e} . \quad (4)$$

The first term in Eq. (4) is the inertia of the electron azimuthal motion and is the dominant convective contribution. Then, the collisional approximation requires

$$\omega_e^{-1} |dv_{\theta e}/dx| \ll 1 \quad (5)$$

and reduces Eq. (4) to

$$v_{\theta e}/v_{xe} \simeq -\omega_e/\nu_e . \quad (6)$$

The equation for the electron internal energy reads

$$\nabla\cdot\left(\tfrac{3}{2}n_eT_e\mathbf{v}_e+\mathbf{q}_e\right)=-n_eT_e\nabla\cdot\mathbf{v}_e-\mathbf{v}_e\cdot\mathbf{R}_e-\nu_in_e\alpha_iE_i. \tag{7}$$

Here, $\mathbf{q}_e$ is the electron heat conduction, $\mathbf{v}_e\cdot\mathbf{R}_e \simeq m_en_e\nu_e v_{\theta e}^2$ is the Joule heating (we assumed $v_{xn}\ll v_{xi}\sim v_{xe}\ll v_{\theta e}$), and the last term on the right-hand side accounts for ionization and excitation losses; E_i is the ionization energy, α_i is the ionization cost factor (taking into account excitation and multistep ionization), and $\nu_i=n_nR_i(T_e)$ is the ionization frequency. Only single ionization will be considered, Dugan's formula (cited in Ref. 12)

$$\alpha_i(T_e)\simeq 2+\frac{1}{4}\exp\frac{2E_i}{3T_e},$$

will be used, and the expression for the ionization rate, $R_i(T_e)$, will be taken from Ref. 1.

Equation (7) for the internal energy identifies clearly the effects contributing to the electron heating. Thus, it is more adequate to use than the equation for the electron total energy, where the contributions to the internal and mechanical energy are mixed. Indeed, the equation for the mechanical energy comes from Eqs. (3) and (4),

$$n_ev_{xe}\frac{d}{dx}\left(\frac{1}{2}m_ev_{\theta e}^2\right)=-v_{xe}\frac{d}{dx}n_eT_e-\nu_em_en_ev_{\theta e}^2+en_ev_{xe}\frac{d\phi}{dx}. \tag{8}$$

Notice that the term on the left-hand side corresponds to the convective contribution, and *must* be neglected when the collisional limit (6) is used.

Tahara *et al.*[14] incur an inconsistency by including the electron mechanical energy in the total energy equation while using, at the same time, the collisional approximation in the momentum equation. Barral *et al.*[15] proposed a nonstationary model which, in the stationary limit, reduces to Eqs. (3), (4), and (7). However, (i) in the nonstationary formulation, they omit the temporal term $\partial v_{\theta e}/\partial t$ associated to the azimuthal inertia, and (ii) it is unclear whether they really include the inertia term in the numerical integration, since they omit explicitly a boundary condition for $v_{\theta e}$.

To close the equations for electron dynamics, a transport equation is needed for $\mathbf{q}_e$. In the collisional approximation, that equation is[19]

$$\tfrac{5}{2}n_eT_e\nabla T_e+e\mathbf{q}_e\wedge\mathbf{B}+m_e\nu_e\mathbf{q}_e\simeq 0,$$

from where the azimuthal and axial components of $\mathbf{q}_e$ satisfy

$$0\simeq-\omega_eq_{xe}-\nu_eq_{\theta e}, \tag{9}$$

$$0\simeq-\frac{5}{2m_e}\frac{dT_e}{dx}+\omega_eq_{\theta e}. \tag{10}$$

The resulting equation for q_{xe} coincides with the one obtained by Fife from the postulate of equal diffusitivities for heat and mass transport.[12]

B. Quasineutral equations

Equations for ions and neutrals are the same as in Model I. Adding them to the above collisional model for the electrons, the quasineutral plasma satisfies

$$\frac{d\Gamma_i}{dx}=\frac{d\Gamma_e}{dx}=\frac{d\Gamma_n}{dx}=An_e\nu_i, \tag{11}$$

$$v_{xn}=\text{const}, \tag{12}$$

$$\frac{1}{A}\frac{d}{dx}(m_iv_{xi}\Gamma_i)=-en_e\frac{d\phi}{dx}+m_in_e\nu_iv_{xn}-\frac{dn_eT_i}{dx}, \tag{13}$$

$$0=-\frac{d}{dx}n_eT_e+en_e\frac{d\phi}{dx}-\nu_dm_en_ev_{xe}, \tag{14}$$

$$\frac{1}{A}\frac{d}{dx}\left(\frac{3}{2}T_e\Gamma_e+Aq_{xe}\right)=-n_eT_e\frac{dv_{xe}}{dx}+\nu_dm_en_ev_{xe}^2-\nu_in_e\alpha_iE_i, \tag{15}$$

$$\frac{dT_e}{dx}=-\frac{2m_e\nu_d}{5n_eT_e}q_{xe}. \tag{16}$$

Here, symbols are conventional or were defined already in Ref. 1. In Eq. (11), $\Gamma_\alpha=An_\alpha v_{x\alpha}$ ($\alpha=i,e,n$) are the species flows, which satisfy

$$\Gamma_i(x)+\Gamma_n(x)=\text{const}=\dot{m}_A/m_i,$$

$$\Gamma_i(x)-\Gamma_e(x)=\text{const}=I_d/e.$$

Related parameters of interest when studying the discharge are the current parameter $i_d=m_iI_d/e\dot{m}_A$, the ionized flux fraction $\eta_i(x)=m_i\Gamma_i(x)/\dot{m}_A$, and the utilization efficiency $\eta_u=\eta_{i\infty}$. Equations (6) and (9) have been used to eliminate $v_{\theta e}$ and $q_{\theta e}$ in the Ohm law (14) and the Fourier law (16), respectively. The axial discharge is governed by two effective frequencies: the axial diffusion frequency for the magnetized electrons, $\nu_d=\omega_e^2/\nu_e$, and the ionization frequency $\nu_i=n_nR_i(T_e)$. The area $A(x)$ and thickness $h(x)$ of the annular cross section of the plasma jet, remain constant within the channel and satisfy

$$\frac{d}{dx}\ln A=\frac{d}{dx}\ln h=\frac{2}{h}\tan\delta=\frac{2c_{\text{pl}}}{v_{xi}h}, \tag{17}$$

in the plume; here $\delta(x)$ is the mean semiangle of divergence of the plume and c_{pl} is the velocity of lateral expansion of the plume, which we will define below.

To close the set of Eqs. (11)–(17), an equation for the ion temperature is needed. For the moment, we apply the ansatz $T_i\ll T_e$, which allows us to neglect the ion pressure in Eq. (13) and thus to drop T_i from the equations. The ion temperature and the validity of the ansatz will be discussed later.

The quasineutral model applies between the entrance to the anode sheath (point B) and $x=+\infty$, except for a discontinuity on the electron current at the neutralization surface (point P). The anode sheath must be solved separately, in its own natural scale (the Debye length), and provides boundary conditions for the quasineutral model at point B.

III. MODEL INTEGRATION

A. Singular/sonic points

Solving Eqs. (11)–(17), with $T_i=0$, for the spatial derivatives we obtain a matrix relation of the form

$$(1-M^2)d\mathbf{Y}/dx=\mathbf{F}(\mathbf{Y}), \tag{18}$$

where $M=v_{xi}(T_e/m_i)^{-1/2}$ is the isothermal Mach number for the ion axial flow, $\mathbf{Y}$ groups the eight plasma variables $(n_e,\ n_n,\ v_{xi},\ v_{xe},\ v_{xn},\ T_e,\ q_{xe})$, and ϕ, and $\mathbf{F}(\mathbf{Y})$ is a regular function. In particular, the scalar equation for v_{xi} can be written as

$$\frac{dv_{xi}}{dx}=\nu_i-v_{xi}\left[\frac{G}{T_e(1-M^2)}+\frac{1}{A}\frac{dA}{dx}\right]$$

with

$$G=-\nu_d m_e v_{xe}\left(1-\frac{2q_{xe}}{5n_eT_ev_{xe}}\right)-\nu_i m_i(2v_{xi}-v_{xn})+m_iv_{xi}^2\frac{d\ln A}{dx}. \tag{19}$$

Sonic points, $M=\pm 1$, are singular points of Eq. (18). Notice that the definition of the Mach number in Model II does not include the specific heat ratio 5/3 of Model I, and function G is different too. As in Ref. 1 we will look for solutions with a regular sonic transition,

$$G_S=0 \quad \text{and} \quad M_S=1 \tag{20}$$

inside the thruster (point S in Fig. 1) and a supersonic plasma flow at the thruster exhaust.

B. Anode sheath

The Debye sheath attached to the anode (region AB in Fig. 1) completes the 1D model of the channel and defines boundary conditions at point B for the quasineutral equations. Under usual conditions, the sheath is electron-repelling and the space-charge field adjusts the potential jump in the sheath, $\phi_{AB}\equiv\phi_B-\phi_A>0$, to a value such that the flow of electrons reaching the anode is equal to the diffusive flow coming from the quasineutral channel.

In the distinguished limit $\lambda_D/L_c\to 0$, the problem in the sheath reduces to collisionless, conservation equations. In particular, particle and energy flows are constant. Assuming a quasi-Maxwellian electron distribution with temperature T_{eB}, electron magnitudes at points A and B are related by

$$(n_ev_{xe})_B=-\frac{1}{4}n_{eB}\exp\frac{-e\phi_{AB}}{T_{eB}}\sqrt{\frac{8T_{eB}}{\pi m_e}},$$
$$(\tfrac{5}{2}n_ev_{xe}T_e+q_{xe})_B=(2T_{eB}+e\phi_{AB})(n_ev_{xe})_B. \tag{21}$$

The matching of this ion-attracting sheath with the quasineutral plasma at point B requires the plasma to verify the Bohm condition

$$M_B=-1, \tag{22}$$

which states that the ions must flow into the sheath with the plasma local sound speed. Using Eqs. (21) the potential jump across the sheath satisfies

$$\frac{e\phi_{AB}}{T_{eB}}=\ln\sqrt{\frac{T_{eB}}{2\pi m_ev_{xeB}^2}}=\ln\left(\sqrt{\frac{m_i}{2\pi m_e}}\left|\frac{\Gamma_{iB}}{\Gamma_{eB}}\right|\right), \tag{23}$$

and the electron energy flux deposited by conduction into the anode sheath is

$$q_{xeB}=(n_ev_{xe}T_e)_B\left(\frac{e\phi_{AB}}{T_{eB}}-\frac{1}{2}\right). \tag{24}$$

C. Boundary conditions

Following Ref. 1 the appropriate velocity for the plume radial expansion is the plasma sound velocity at the thruster exhaust,

$$c_{\rm pl}=\sqrt{T_{eE}/m_i}. \tag{25}$$

Equations (11)–(16) need eight boundary conditions. Seven of them are similar to Model I and there is one additional condition for q_{xe}. The eight conditions are as follows.

(i) and (ii) The injected flow and the velocity of neutrals at the anode, $\dot m_A$ and $v_{nA}(=v_{nB})$, are known.

(iii) The electron temperature at the neutralization surface, T_{eP}, is known.

(iv) The discharge voltage, $V_d=\phi_A-\phi_P$, is known.

(v) There is a regular sonic point inside the channel characterized by Eq. (20).

(vi)–(viii) The matching with the anode sheath yields conditions (22)–(24).

D. Integration procedure

From the preceding equations and conditions, it turns out that the quasineutral model requires input parameters of different kinds. There are design parameters $(A_c,\ L_c)$, control parameters $(V_d,\ B(x),\ \dot m_A)$, plasma parameters $(T_{eP},\ v_{nB})$, and empirical parameters $(L_{cat},\ \alpha_{\rm ano})$. The main output parameters are the discharge current I_d, the thrust F, and the thrust efficiency η, the two last ones to be defined later. Other output parameters of interest are the position of the sonic point, x_S, the divergence angle at the thruster exhaust, δ_E, and several partial efficiencies.

Plasma equations are nondimensionalized as in Model I; hereafter, an upper tilde will indicate dimensionless variables. Then, equations are integrated with Runge–Kutta plus shooting routines from point S towards points B and P independently. This means that plasma parameters at point S are used as input parameters of integration. A Taylor expansion solves the indeterminacy $G_S/(1-M_S^2)=0/0$ and yields the slopes of plasma variables at point S. Using Eq. (19), the regularity condition (20) can be expressed as

$$\frac{\nu_i m_i}{\nu_d m_e}=\frac{-v_{xe}+2q_{xe}/(5n_eT_e)}{2v_{xi}-v_{xn}}. \tag{26}$$

It is easily seen that this equation relates η_{iS} to $\tilde T_{eS}$, $\tilde q_{xeS}$, and i_d. The integration uses these three quantities as input parameters instead of the natural ones, $\tilde T_{eP}$, $\tilde q_{xeB}$, and $\tilde V_d$.

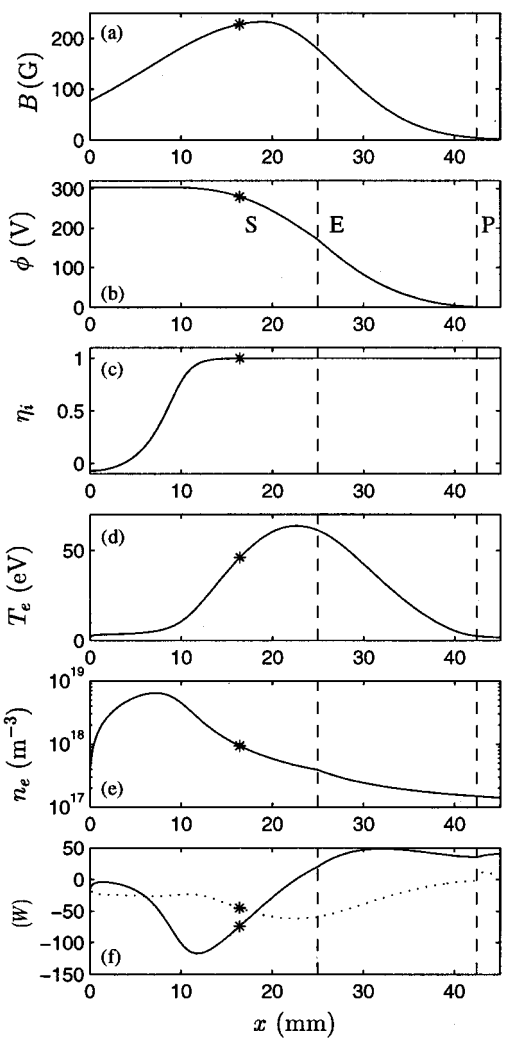

FIG. 2. Axial structure of the plasma for xenon, $L_c=25$ mm, $L_{cat}=17.4$ mm, $A_c=45$ cm^2, $\dot{m}_A=5.3$ mg/s, $V_d=298$ V, $T_{eP}=2.5$ eV, $16\alpha_{ano}\simeq 0.068$, and $B(x)$ as shown in (a). Output parameters: $I_d=4.51$ A, $F=0.108$ N, $\eta=80.8\%$, $\eta_{iB}=-7.1\%$, $\phi_{AB}\simeq 4.4$ V, $x_S=16.4$ mm, $\delta_E\simeq 25.7°$. The vertical, dashed lines are the thruster exhaust and the neutralization surface; the asterisk situates point S. In (f) the solid line corresponds to the conductive electron power, Aq_{xe}, and the dashed line to the convective one, $A\frac{5}{2}T_e n_e v_{xe}$.

As a consequence, an iteration is needed to reproduce the desired operating conditions. An additional difficulty of Model II, compared to Model I, is that the solutions departing from point S do not converge easily to the boundary conditions at point B. Thus, we were forced to launch solutions from points S and B separately and to match them at an intermediate point.

Once the region between points B and P is solved the solution is continued to $x=+\infty$ by just changing the condition $\Gamma_{eP^-}=\Gamma_{iP}-I_d/e$ to $\Gamma_{eP^+}=\Gamma_{iP}$.

IV. ANALYSIS OF THE SPATIAL SOLUTION

A. Axial structure of the discharge

Figure 2 shows the axial profiles of main plasma variables for an SPT-100 type of thruster; design and control parameters are given in the figure caption. The discharge presents a similar structure to the one obtained in Model I and sketched in Fig. 1, consisting of the anode sheath, the reverse-flow region, the ionization layer, the internal acceleration region, and the plume. However, heat conduction introduces some differences of relevance. First, there is the desired smoothing of the temperature profile, with a peak temperature around 60 eV, instead of the 90 eV of Model I. Second, the sharp transition between the reverse-flow and ionization regions found in Model I has been smoothed too, yielding a shorter reverse-flow region here. Notice that a simple dimensional analysis of Eqs. (14)–(16) suggests that heat conduction is of the same order as convective energy flow. Figure 2(f) shows that heat conduction (which changes sign near the channel exhaust) is even larger than the convective flow in certain regions.

Plasma equations and boundary conditions force an almost monotonic profile of q_{xe} between B and S. Therefore, q_{xe} at point S is negative and the point of maximum temperature (i.e., $q_{xe}=0$) is placed downstream of point S, near the channel exit. Function G of Model II, Eq. (19), shows that the energy balance allowing the regular sonic transition at point S involves losses by ionization, Joule heating, and heat conduction. However, it turns out that point S is practically in the acceleration region and the ionization contribution to the above balance is small, in marked contrast with Model I. For the case of Fig. 2, the point with $q_{xe}=0$ is at $x\simeq 22.6$ mm, the sonic point is at $x_S\simeq 16.4$ mm, about 1 mm downstream of the main ionization zone; thus, it still seems adequate to take point S as the practical end of the ionization layer.

From Fig. 2(b), the sheath potential drop is $\phi_{AB}=4.4$ V, the potential increase in the reverse-flow region is just $\phi_{BD}\simeq 1$ V and the potential drop in the ionization layer is $\phi_{DS}\simeq -24.1$ V. Since the temperature at the sonic point is $T_{eS}\sim 46.2$ eV, one has $\phi_{BS}\simeq -T_{eS}/2$, which means that equation $m_i v_{xi}^2/2-e\phi\simeq$ const is satisfied approximately, and the dispersion of ion velocities is small, a conclusion to be confirmed later.

The typical magnitudes of the reverse-flow plus ionization regions can be obtained from a dimensional analysis of the plasma equations. Taking $\alpha_i E_i$ (~ 30 eV) as the distinguished energy there, the length of region AS, L_{AS}, follows the known scaling[20]

$$L_{AS}\sim \ell_e\sqrt{\nu_e/\nu_i},\quad \ell_e=\omega_e^{-1}\sqrt{\alpha_i E_i/m_e}; \tag{27}$$

in Fig. 2 one has $\ell_e\sim 1$ mm and $\nu_e/\nu_i\sim 200$. The average electron density in region AS comes from the ion continuity equation, $n_e=\dot{m}_A/(m_i A_c \nu_i L_{AS})$.

The structure of the internal and external acceleration regions (region SP in Fig. 1) is simpler because ionization is negligible there. The quasineutral model simplifies to the conservation relations,

$$\Gamma_\alpha=\text{const},\quad m_i v_{xi}^2/2+e\phi=\text{const},$$
$$5T_e/2-e\phi+q_{xe}/n_e v_{xe}=\int T_e d\ln A, \tag{28}$$

plus Eqs. (14) and (16) for electron momentum and heat conduction. These two last equations show that

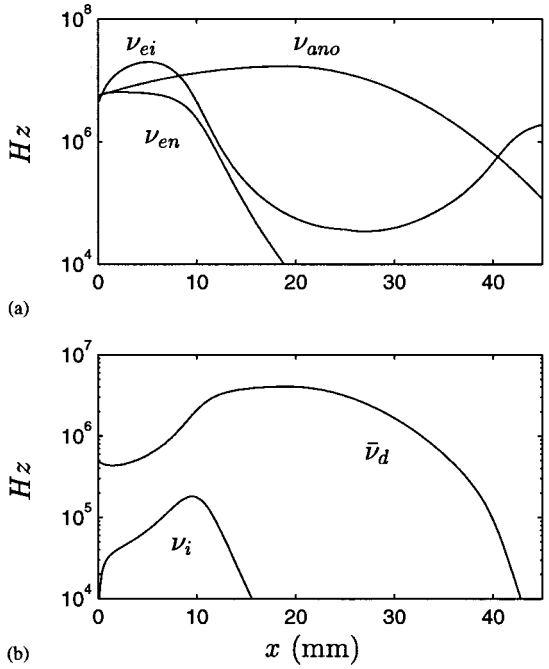

FIG. 3. For the solution of Fig. 2: (a) contributions of different processes to the total electron collision frequency ν_e; and (b) ionization frequency, ν_i, and axial electron diffusion frequency, $\overline{\nu_d}=\nu_d m_e/m_i$.

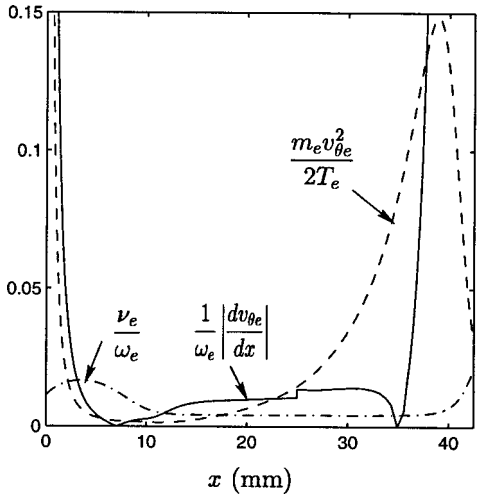

FIG. 4. Profiles of the inverse Hall parameter, ν_e/ω_e, the drift-to-internal energy ratio, $m_e v_{\theta e}^2/2T_e$, and the convective-to-magnetic time ratio, $\omega_e^{-1}|dv_{\theta e}/dx|$, for the case of Fig. 2.

$\int(-v_{xe})m_e\nu_d\,dx$ is the adequate integration variable for the acceleration regions. Quasineutrality and flow conservation state that the electrons counterflow with a velocity $v_{xe}=-(i_d/\eta_u-1)v_{xi}$. Adding to this the fact that (i) the ion flow is mostly supersonic and (ii) most of the voltage drop takes place in the region SP, the integration of Eq. (14) yields

$$\sqrt{\frac{2eV_d}{m_i}}\sim\int_S^P\left(\frac{i_d}{\eta_u}-1\right)\frac{m_e\omega_e^2}{m_i\nu_e}dx. \tag{29}$$

This expression suggests

$$V_d^{1/2}\propto(i_d-1)L_{SP}B_{\max}^2/\nu_e, \tag{30}$$

with $L_{SP}=x_P-x_S$, as one of the main scaling laws among the thruster parameters when it operates efficiently.

Kim[5] derived a law similar to Eq. (30). Then, assuming that (i) $L_{SP}\simeq$const (for a given geometry), (ii) $(i_d-1)\simeq$const, and (iii) $\nu_e\sim V_d^{1/2}h_c^{-1}$ (from an estimate based in the dominance of wall collisions), he concluded that optimum operation required $B_{\max}\propto V_d^{1/2}$. Curiously, when anomalous diffusion dominates one has $\nu_e\sim\alpha_{\text{ano}}B_{\max}$ and the scaling law $B_{\max}\propto V_d^{1/2}$ still holds, provided that the condition $(i_d-1)\simeq$const applies. We come back to this scaling law in Sec. VI B.

Figure 3(a) compares the contributions of different collision terms to the electron collision frequency ν_e. The main conclusion is that anomalous diffusion provides the main contribution downstream of the ionization layer, a result supported experimentally.[2,21] However, we still adjust α_{ano} empirically to obtain a satisfactory solution; the value we used is similar to the one taken by Fife,[12] and is almost one order of magnitude smaller than the classical value of Bohm. Also, Fig. 3(a) shows that $e-i$ collisions dominates over $e-n$ collisions in the rear part of the channel; this is due to the high electron density and low electron temperature arising when the ionization region is thin. Figure 3(b) depicts the two frequencies governing the axial discharge, ν_i and $\overline{\nu_d}=\nu_d m_e/m_i$ [with the mass ratio in $\overline{\nu_d}$ coming from the dimensional analysis of Eqs. (11)–(16)]. The plots show that $\nu_i\ll\overline{\nu_d}$ even at the peak of ν_i, which explains the difficulty in carrying out a simple asymptotic analysis of the reverse-flow plus ionization regions.

B. Inertial effects on electrons

We evaluate now the assumptions of closed-drift and collisional electron dynamics. Figure 4 plots, for the case of Fig. 2, three parameters related to electron dynamics: the inverse Hall parameter, the drift-to-internal energy ratio, and the magnetic-to-convective time ratio. We see, first, that the closed-drift approximation, Eq. (2), is verified in the whole domain, even near the cathode, where the magnetic field is vanishing. However, the collisional approximation, Eq. (5), fails in the vicinities of anode and cathode. Electron convective effects around the anode come from $v_{xe}\propto v_{xi}$ and the acceleration of the plasma having to meet the Bohm condition at point B. These effects are rather local and we believe they are not significant globally. On the contrary, the inertia effects in the plume could have more impact in the plasma discharge since they are less localized and the magnetic field becomes residual there. From Eq. (4), one has

$$\frac{v_{xe}}{v_{\theta e}}\simeq-\frac{\nu_e}{\omega_e+dv_{\theta e}/dx}\sim-\frac{\nu_e}{\omega_e}\left(1-\frac{1}{\omega_e}\frac{dv_{\theta e}}{dx}\right), \tag{31}$$

with $dv_{\theta e}/dx<0$ in the plume, yielding thus a larger value of $v_{xe}/v_{\theta e}$ than the collisional approximation. This can be interpreted as an extra collisionality and could be an important and independent contribution to the overall anomalous diffusion. However, without solving the coupled equations

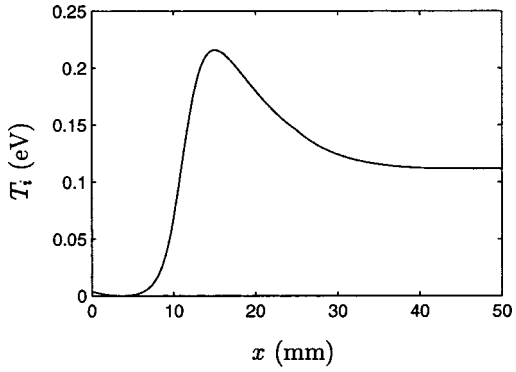

FIG. 5. Profile of the ion temperature for the case of Fig. 2.

(3) and (4) together with the other ones, it is difficult to predict the overall effect of the convective term on the discharge characteristics.

In spite of the large values reached by the convective azimuthal term, Fig. 4 shows that the drift energy remains small in the whole domain. The explanation lies in the azimuthal inertia term of Eq. (4) being balanced by the azimuthal component of the Lorentz force, which yields no contribution to the drift energy. In any case, $v_{\theta e}$ is very sensitive to the local values of the magnetic and electric fields, and relatively small variations of these magnitudes could make $m_e v_{\theta e}^2/2T_e \sim 1$ locally.[6] Were this the case, the drift energy should be taken into account to compute the ionization rate, R_i.

C. Ion temperature

The evolution equation for the ion temperature is

$$v_{xi}\frac{d}{dx}\frac{3}{2}T_i = -\frac{T_i}{A}\frac{d}{dx}Av_{xi} + \nu_i\left[\frac{1}{2}m_i(v_{xi}-v_{xn})^2 + \frac{3}{2}(T_n - T_i)\right], \tag{32}$$

where T_n is the temperature of neutrals. Equation (32) requires a boundary condition for T_i and, at the same time, introduces a new singular point at $v_{xi}=0$. The correct boundary condition for a regular solution comes from making zero the right-hand side of Eq. (32) at $v_{xi}=0$: this yields $T_i = (3T_n + m_i v_{xn}^2)/5$. Again a Taylor-expansion problem must be solved to determine the value of dT_i/dx for a regular crossing.

Figure 5 plots $T_i(x)$, obtained from the integration of Eq. (32) using $v_{xi}(x)$ and $A(x)$ from the cold-ion solution of Fig. 2, and $T_n/T_e \to 0$. It confirms that T_i is totally negligible and the ion beam is nearly monoenergetic. Clearly, the small value of T_i and the drawback of a new singular point at $v_{xi}=0$ makes it inadvisable to add Eq. (32) to the set of Eqs. (11)–(17).

The low ion temperature is due to the short ionization region and the absence of lateral recombination. The experimental retarding potential analyzer data show that $T_i \sim 2-3$ eV at exit. The discrepancy might be related to the spreading of the ionization zone when there is wall recombination; ion–ion and ion–neutral collisions could contribute too.

V. THRUST AND EFFICIENCY

A. Thrust

The electrostatic interaction between ions and electrons plus the magnetic forces on the electrons are the mechanisms by which plasma thrust is transferred to the solids parts of the engine. Since the magnetic field extends some distance outside the chamber and the plasma plume presents some radial divergence, neither the momentum thrust of the plasma at the chamber exhaust (point E) nor in the far plume (point ∞) evaluate accurately the thrust.

Assuming the engine to be at rest by some thrust balance device and zero external pressure, the axial momentum balance for the system constituted by the thruster plus the internal plasma yields

$$F = F_{pE} + F_{m,\mathrm{ext}}, \tag{33}$$

where F is the thrust (exerted on the thruster balance),

$$F_p(x) = (m_i n_i v_{xi}^2 + m_i n_n v_{xn}^2 + n_e T_e)A(x) \tag{34}$$

is the total axial momentum of the plasma at a given axial section, and

$$F_{m,\mathrm{ext}} = \int_E^\infty e n_e v_{\theta e} B A(x)\,dx \tag{35}$$

is the external thrust due to the magnetic force on the electrons *in the plume*. Therefore, the leakage of the magnetic field outside the thruster channel yields a contribution to the thrust, which is a unique characteristic of this type of electric thrusters.

From Eqs. (6), (13), and (14), the axial momentum of the whole plasma satisfies

$$dF_p/dx = n_e T_e\, dA/dx + e n_e v_{\theta e} B A. \tag{36}$$

Integrating Eq. (36) along the plume and using Eq. (33) one has

$$F = F_{p\infty} - D_{\mathrm{ext}}, \tag{37}$$

with $D_{\mathrm{ext}} = \int_E^\infty n_e T_e\, dA$ the drag contribution due to the plume lateral expansion. Expressions (33) and (37) yield the difference between the actual thrust and the momentum thrust at points E and ∞. One has $F_{p\infty} - F_{pE} = F_{m,\mathrm{ext}} + D_{\mathrm{ext}}$, which means that the external acceleration of the ions is transferred only partially to thrust (via ion–electron electrostatic interaction plus electron–thruster magnetic interaction). A relevant point is that were the magnetic field zero outside the thruster, all external acceleration would go to plume radial expansion. For the case of Fig. 2 we have that the contribution of the external magnetic field amounts to $F_{m,\mathrm{ext}}/F \simeq 15.8\%$ whereas the external acceleration of ions is $(F_{p\infty} - F_{pE})/F \simeq 19.7\%$.

B. Thrust efficiency

The thrust efficiency is defined as

$$\eta = F^2/2\dot{m}_A I_d V_d, \tag{38}$$

and is conveniently factorized into four terms, $\eta = \eta_u \eta_d \eta_e \eta_o$, where η_u is the propellant utilization, and

$$\eta_d = \frac{I_{i\infty}}{I_d} \equiv \frac{\eta_u}{i_d}, \quad \eta_e = \frac{m_i v_{xi\infty}^2}{2eV_d}, \quad \eta_o = \frac{F^2}{(\Gamma_i m_i v_{xi})_\infty^2}, \tag{39}$$

are efficiencies for discharge, beam-energy, and other effects (plume expansion, anode sheath,...), respectively. For the case of Fig. 2, one has $\eta_u \simeq 100\%$, $\eta_d \simeq 85.6\%$, $\eta_e \simeq 101.4\%$, $\eta_o \simeq 93.4\%$, and $\eta \simeq 81.1\%$; the thin ionization region and the fact that the maximum voltage is not at point A but at $v_{xi}=0$ are responsible of $\eta_e > 100\%$. Notice that the definition of η is based in the anode mass flow and does not include the power spent in the magnetic circuit.

The discharge efficiency is the main factor reducing the thrust efficiency. The relation between η_d (or i_d) and the ionization losses is deduced from the energy balance for the whole plasma. From the model equations, the energy balance for the plasma is

$$I_d V_d = \sum_{\alpha=i,e,n} (P_{\alpha\infty} - P_{\alpha A}) + P_{\text{ion}} \tag{40}$$

with

$$P_\alpha = \Gamma_\alpha (\tfrac{1}{2} m_\alpha v_{x\alpha}^2 + \tfrac{5}{2} T_\alpha) + q_{x\alpha} A \tag{41}$$

the energy flow rate of each species, and

$$P_{\text{ion}} = \int_A^\infty \nu_i \alpha_i E_i n_e A \, dx \tag{42}$$

the ionization losses. Grouping in Eq. (40) the nondominant contributions into P_{rest}, the energy balance becomes

$$I_d V_d = P_{i\infty} + P_{\text{ion}} + P_{\text{rest}};$$

in Fig. 2, one has $P_{\text{ion}}/I_d V_d \simeq 9.3\%$ and $P_{\text{rest}}/I_d V_d \simeq 3.7\%$ (with $q_{xe\infty}$ the main contribution to P_{rest}). From the efficiency definitions and a cold ion beam one has

$$\frac{P_{\text{ion}} + P_{\text{rest}}}{I_d V_d} \simeq 1 - \eta_e \eta_d \sim 1 - i_d^{-1}, \tag{43}$$

which relates directly the discharge efficiency to the relative ionization losses, and complements the scaling law (30).

VI. THRUSTER PERFORMANCE

A. Domain of stationary solutions

In Ref. 1 we suggested that the parametric domain of stationary solutions was restricted to the range $\eta_{iB} \leqslant 0$ (i.e., $\Gamma_{iB} \leqslant 0$). We argued that beyond the parametric line $\eta_{iB}=0$ the plasma is unable to provide the ion back-flow needed to keep plasma quasineutrality near the anode, making unclear the possibility of a stationary response. In addition, the assumption of an electron-repelling sheath at the anode further restricts the minimum value of $|\eta_{iB}|$. The anode sheath vanishes when $\phi_{AB}=0$, which, from Eq. (23), corresponds to

$$\frac{-\eta_{iB}}{i_d - \eta_{iB}} = \sqrt{\frac{2\pi m_e}{m_i}}, \quad v_{xeB} = -\sqrt{\frac{T_{eB}}{2\pi m_e}}. \tag{44}$$

Since $i_d \sim 1$, the sheath disappears for $\eta_{iB} \sim -\sqrt{2\pi m_e/m_i} \sim -10^{-2}$. Although it is possible to extend Model II to treat cases with no electron-repelling sheath, here we take the case of sheath collapse as the practical limit of existence of stationary solutions. There are two reasons for this: first, the limit $\eta_{iB}=0$ is very close; and second, Eq. (44) and Fig. 4 show that, when $\phi_{AB}=0$, the electron velocity is large, formally beyond the limit of validity of the collisional model.

An important novelty of Model II with respect to Model I is that heat conduction introduces an upper restriction on $|\eta_{iB}|$. This comes from the Bohm condition at point B. To have $dv_{xi}/dx|_B \geqslant 0$ requires $G_B \geqslant 0$, which using Eq. (19) and $\nu_{iB} \simeq 0$ means $q_{xeB} \leqslant (5/2)(n_e T_e v_{xe})_B$. For $G_B < 0$, the reverse ion velocity reaches a minimum subsonic value at an intermediate point of region BD and the sonic condition at point B cannot be met. Physically, this would mean the impossibility to establish a stationary sheath at the anode and a possible oscillatory response of the plasma.

Using Eqs. (23) and (24), the domain of solutions of Model II is restricted to

$$0 \leqslant e\phi_{AB}/T_{eB} \leqslant 3, \tag{45}$$

or, in terms of plasma currents (and for xenon), $5\times 10^{-3} \leqslant |I_{iB}|/I_d \leqslant 0.114$.

B. Optimum performance

Figure 6(a) shows the domain of stationary solutions in the plane of input parameters $(V_d, B_{\max})$. Figures 6(b)–6(d) depict the corresponding bands of output parameters. As expected from Eq. (45) the domain of solutions is rather narrow. Figure 6(b) confirms two known features of the specific impulse $I_{\text{sp}} = F/\dot{m}$: first, it is proportional to $V_d^{1/2}$ and, second, it is practically independent of the magnetic field strength (within the high efficiency regime). More interesting issues arise from consideration of the other plots.

Figure 6(a) shows that $B_{\max}$ must increase with V_d to maintain a stationary solution. This same trend is found experimentally for optimum thruster performance, which supports the idea that optimum performance is related to a nonoscillatory response. Then, Fig. 6(a) yields

$$B_{\max} \propto V_d^{5/4} \tag{46}$$

as the approximate scaling law for optimum performance, instead of $B_{\max} \propto V_d^{1/2}$ proposed by Kim. The discrepancy, which might just be due to the effect of wall losses (neglected here), comes from the behavior of $(i_d - 1)$ and L_{AS} in Eq. (30), which Kim assumed independent of V_d, whereas we find

$$i_d - 1 \sim 1 - \eta_d \propto V_d^{-1}, \quad L_{SP} \propto V_d^{1/4}, \tag{47}$$

roughly. These two behaviors can be explained from the plasma equations. First, from the continuity equation, the ionization losses satisfy $P_{\text{ion}} \simeq \alpha_i E_i \Gamma_{iS} = \alpha_i E_i \eta_u \dot{m}_A / m_i$, so

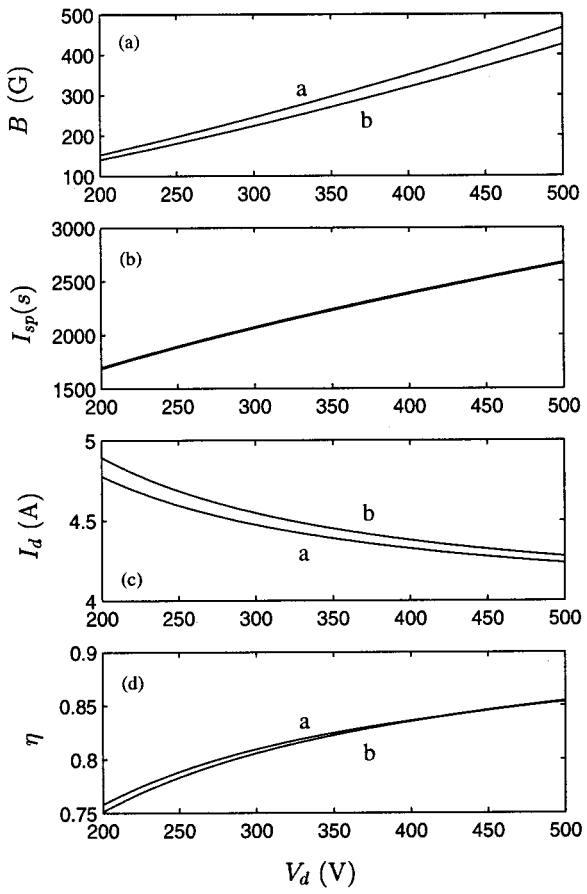

FIG. 6. Band of stationary solutions for input parameters V_d and $B_{\max}$ as in (a) and the rest of input parameters as in Fig. 2; $I_{sp} \equiv F/\dot{m}_A$. Lines a and b correspond to the lower ($\phi_{AB}=0$) and upper ($G_B=0$) restrictions on $|\eta_{iB}|$, respectively.

that P_{ion} is independent of V_d; numerical results show that the marginal term P_{rest} is independent of V_d too. Then, Eq. (43) justifies the above behavior of (i_d-1). Second, for zero wall losses, one expects $T_e \propto V_d$; indeed, our computations yield $T_{e,\max} \simeq V_d/5$, with $T_{e,\max}$ the maximum electron temperature (but we could not find a precise justification of the factor 1/5). This would lead to $T_{eS} \propto V_d$, $\nu_i \propto V_d^{1/2}$, $L_{AS} \propto V_d^{-1/4}$, and, from $L_{SP}+L_{AS}=L_c-L_{cat}$, to the scaling law for L_{SP}. (Of course, these scaling laws must be seen just as dominant trends and valid only within a limited interval of values of V_d.)

The numerical simulations of Blateau *et al.*[22] for a thruster with metallic walls show $B_{\max} \propto V_d$, not far from our result. Experimental data by Manzella *et al.*[23] with a thruster with ceramic walls, fit well with $B \propto V_d^{1/2}$ but η does not increase clearly with V_d. Therefore, our conclusions are that Eqs. (30) and (43) are the main relationships among thruster parameters, whereas the particular scaling laws for the evolution of $B_{\max}$ and $(1-\eta)$ with V_d depend on the thruster operating point and the mechanism dominating energy losses.

VII. CONCLUSIONS

The inclusion of heat conduction in our previous Model I has produced the following changes in both the treatment of the mathematical model and the stationary solutions: (i) a new boundary condition on the heat flow at the anode is needed, (ii) the singular points are modified, (iii) the integration procedure requires more involved iteration routines, and (iv) a new restriction on the parametric domain of stationary solutions has arisen.

Model II recovers an axial structure of the discharge consisting mainly of the reverse-flow plus ionization regions on the rear part of the chamber, followed by the internal and external acceleration regions. The conductive energy transport turns out to be as important as the convective one and is able to smooth the temperature profile. Because of the short ionization region, the ion temperature is found to be negligible, and the transmission of electrostatic energy into the monoenergetic ion beam is very efficient.

The discussion of the inertial effects in the electron dynamics and the electron drift energy has yielded some important conclusions. First, the dominant inertial term comes from the azimuthal electron motion. Second, this term can produce an anomalous-like collisionality in the near plume, which could be important to understand the plasma discharge there; further investigation on this issue seems crucial. Third, the fact that the electron inertia can be significant in a certain region does not imply necessarily that the electron drift energy is important too.

The analysis of the forces contributing to the thrust shows the contribution of the external magnetic fields on the incoming electrons. This external thrust is the main part of the ion acceleration in the plume, which is transmitted to the electrons through the quasineutral electrostatic field. Another part of the ion acceleration goes to the plume radial expansion and does not produce thrust. For our modelization of the magnetic field, the external thrust amounts to near 20%. Therefore, a better knowledge of the profile of the external magnetic field, the approximate position of the neutralization surface, and the external electron dynamics is required in order to compute accurately the discharge characteristics.

The domain of steady solutions given by Model II is narrow, accepting only about a 15% of variation of the discharge voltage (for the rest of parameters given). The agreement of the model with the experimental curves $B_{\max}(V_d)$ for optimum operation of the thruster, suggests that the stationary regime presented here corresponds to the actual regime of efficient operation. Model II proposes $B_{\max} \propto V_d^{5/4}$ and $(1-\eta) \propto V_d^{-1/2}$ as scaling laws for good operation around the nominal design point.

The domain of stationary solutions of Model II is limited by the conditions the plasma must verify at the anode, and more particularly at the electron-repelling sheath formed there. On the one domain end, the Bohm condition at the sheath transition yields an upper bound of the ion reverse flow (and of the discharge voltage), beyond which the reverse flow cannot reach sonic conditions and a stationary sheath cannot be established. This could correspond to reported oscillatory responses for large discharge voltages. At present, we do not see plausible modifications of Model II leading to the extension of the stationary domain beyond the upper bound found here.

The situation is more unclear at the lower bound of the

ion reverse flow (and of the discharge voltage). First, we placed the limits of Models I and II at the vanishing limit of the anode sheath, which takes place for a relative reverse flow of ions of 1%, roughly. A change of boundary conditions at the anode seems enough to extend the domain of stationary solutions until the reverse flow at the anode is zero (or very close to zero). The main reason we had for ignoring that extension was the small parametric range we guessed for this regime. However, the narrow range of solutions we have encountered and the experimental evidence of steady discharges with low applied potentials suggest to analyze that extension.

The high thrust efficiency obtained by Model II (about 75–85 % based in the anode mass flow) and the still high peak temperature, indicate that energy losses due to the plasma interaction with lateral walls (in thrusters with long, ceramic chambers, which are the main reference for our model) are an effect of dominant order, producing energy losses as large as the ionization ones.[5] Preliminary work showed that the effects of the radial plasma-wall interaction can be included in axial models of the discharge through three forcing terms.[24] Although the quantitative plasma response is expected to be affected substantially by the radial interaction, the restrictions on the ion reverse flow and the domain of steady solutions are going to be as severe (qualitatively) as in the present model, since the radial forcing terms do not affect the plasma conditions at the anode. Finally, the inclusion of wall losses will also provide more insight on the exponent p of the scaling law $B_{\max} \propto V_d^p$ for optimum performance, which is estimated between 1/2 and 5/4 depending on the authors.

ACKNOWLEDGMENT

This work was supported by the European Office for Aerospace Research and Development, under Contract No. F61775-01-WE070 (supervised by Dr. Ingrid Wysong).

[1] E. Ahedo, P. Martínez-Cerezo, and M. Martínez-Sánchez, Phys. Plasmas **8**, 3058 (2001).
[2] G. Janes and R. Lowder, Phys. Fluids **9**, 1115 (1966).
[3] A. Bishaev and V. Kim, Sov. Phys. Tech. Phys. **23**, 1055 (1978).
[4] G. Guerrini, C. Michaut, M. Dudeck, A. Vesselovzorov, and M. Bacal, *25th International Electric Propulsion Conference, Cleveland, OH* (Electric Rocket Propulsion Society, Cleveland, OH, 1997), IEPC 97-053.
[5] V. Kim, J. Propul. Power **14**, 736 (1998).
[6] J. M. Haas and A. D. Gallimore, *36th Joint Propulsion Conference, Huntsville, Alabama* (American Institute of Aeronautics and Astronautics, Washington, DC, 2000), AIAA 2000-3422.
[7] K. Komurasaki, K. Mikami, and Y. Arakawa, J. Propul. Power **11**, 1317 (1995).
[8] A. Fruchtman and N. Fisch, *34th Joint Propulsion Conference, Cleveland, OH* (American Institute of Aeronautics and Astronautics, Washington, DC, 1998), AIAA 98-3500.
[9] J. Boeuf and L. Garrigues, J. Appl. Phys. **84**, 3541 (1998).
[10] E. Ahedo, P. Martínez, and M. Martínez-Sánchez, *36th Joint Propulsion Conference, Huntsville, Alabama* (American Institute of Aeronautics and Astronautics, Washington, DC, 2000), AIAA 2000-3655.
[11] E. Ahedo, P. Martínez-Cerezo, J. Gallardo, and M. Martínez-Sánchez, *SP-476: Proceedings of the 7th Spacecraft Charging Technology Conference* (European Space Agency, Noordwijk, the Netherlands, 2001), pp. 539–544.
[12] J. M. Fife, Ph.D. thesis, Massachusetts Institute of Technology, 1998.
[13] E. Ahedo, P. Martínez-Cerezo, and M. Martínez-Sánchez, *37th Joint Propulsion Conference, Salt Lake City, UT* (American Institute of Aeronautics and Astronautics, Washington, DC, 2001), AIAA 2001-3323.
[14] H. Tahara, D. Goto, T. Yasui, and T. Yoshikawa, *27th International Electric Propulsion Conference, Pasadena, CA* (Electric Rocket Propulsion Society, Cleveland, OH, 2001), IEPC 01-42.
[15] S. Barral, K. Makowski, Z. Peradzynski, N. Gascon, and M. Dudeck, *27th International Electric Propulsion Conference, Pasadena, CA* (Electric Rocket Propulsion Society, Cleveland, OH, 2001), IEPC 01-27.
[16] V. Fedotov and A. Ivanov, Phys. Plasmas **6**, 4360 (1999).
[17] D. Bohm, *The Characteristics of Electrical Discharges in Magnetic Fields* (MacGraw-Hill, New York, 1949), p. 77.
[18] A. Bugrova, A. Morozov, and V. K. Kharchevnikov, Sov. J. Plasma Phys. **16**, 849 (1990).
[19] J. Bittencourt, *Fundamentals of Plasma Physics* (Pergamon, Oxford, 1986).
[20] V. Zhurin, H. Kaufman, and R. Robinson, Plasma Sources Sci. Technol. **8**, R1 (1999).
[21] N. Meezan and M. Capelli, *36th Joint Propulsion Conference, Huntsville, AL* (American Institute of Aeronautics and Astronautics, Washington, DC, 2000), AIAA 2000-3420.
[22] V. Blateau, M. Martínez-Sánchez, O. Batishchev, and J. Szabo, *27th International Electric Propulsion Conference, Pasadena, CA* (Electric Rocket Propulsion Society, Cleveland, OH, 2001), IEPC 01-37.
[23] D. Manzella, D. Jacobson, and R. Jankovsky, *37th Joint Propulsion Conference, Salt Lake City, UT* (American Institute of Aeronautics and Astronautics, Washington, DC, 2001), AIAA 2001-3774.
[24] E. Ahedo, P. Martínez-Cerezo, J. Gallardo, and M. Martínez-Sánchez, *27th International Electric Propulsion Conference, Pasadena, CA* (Electric Rocket Propulsion Society, Cleveland, OH, 2001), IEPC 01-17.